Formation of Tethered Nanolayers: Three Regimes of Kinetics

L. S. Penn,* H. Huang, M. D. Sindkhedkar, S. E. Rankin, and K. Chittenden

Department of Chemical and Materials Engineering, University of Kentucky, Lexington, Kentucky 40506-0046

R. P. Quirk, R. T. Mathers, and Y. Lee

Department of Polymer Science, University of Akron, Akron, Ohio 44325-3909

Received April 5, 2002; Revised Manuscript Received June 7, 2002

ABSTRACT: An investigation of the kinetics of tethering of amine functional-ended polystyrene from good solvent to the surface of a solid substrate showed three distinct regimes of kinetics rather than the two predicted by theory. The first regime was fast and appeared to be controlled by diffusion through the solvent, as predicted by theory. The second regime was slow and appeared to be linear in the natural logarithm of time, as predicted by theory. The third regime, not predicted by theory, was one of accelerated tethering (termed by us "layer-assisted tethering"). The third regime, observed for different solvents, different molecular weights, and different temperatures, ended when saturation was reached. We suggest herein an explanation for the observed acceleration.

I. Introduction

A tethered layer, as described in this paper, is a layer composed of polymer chains that are each attached by one end only to the surface of an impenetrable solid. There is ample justification for interest in tethered layers. First, the attachment of polymer molecules to surfaces by means of chemical bonds is an excellent way to fully cover a surface with a permanent, stable layer that is not vulnerable to desorption or displacement. Second, surfaces with any desired physicochemical properties can be designed, in principle, by appropriate choice of monomer chemistry, polymer molecular weight, polymer architecture, and surface attachment density of the chains in the tethered layer.

We stress the difference between tethered layers, which are held to a surface by means of a chemical bond between each polymer chain and the surface, and adsorbed layers, which are held to a surface by means of the physical attraction between multiple segments in each polymer chain and the surface. Adsorbed layers have been studied for decades and are well understood. Tethered layers, on the other hand, are a newer phenomenon. Most experimental studies of tethered layers have focused on the characteristics and behavior of polymer brushes, which are very dense tethered layers, e.g., refs 1−7. Experimental studies focused on the kinetics of tethering are relatively rare,[8−13] and most of them were conducted on diblock copolymer chains in which one block, a nonadsorbing block, was held to the surface by the other block, a strongly adsorbing block.[9−13]

Our ultimate goal is to be able to manipulate the tethering process to form a wide variety of different layers according to design. To do this, we must acquire a thorough understanding of the process. Therefore, the focus of the present paper is the kinetics of formation of tethered layers in which each chain is attached to the solid surface by a chemical bond.

* To whom correspondence should be addressed. Department of Chemical and Materials Engineering, 177 Anderson Hall, University of Kentucky, Lexington, KY 40506-0046. Telephone: 859-257-7897. Fax: 859-323-1929. E-mail: penn@engr.uky.edu.

Theoretical studies on the kinetics of tethering from solution[14,15] and from the melt[16−19] predict distinct regimes of kinetics. We focus on a theory that addresses tethering from solution, since our experiments are tethering from solution. According to theory, tethering in the first regime, during which chains are tethered to the bare, solid surface, is predicted to be relatively rapid and controlled by the center-of-mass diffusion of the chains through the solvent. The second regime is predicted to begin when the chains in the tethered layer are on the verge of overlap, a situation that creates an energy barrier to the diffusion of subsequent chains to the surface. According to theory, as time goes on, subsequent chains do surmount the energy barrier, adding to the tethered layer and increasing the energy barrier to diffusion even more. The progressively increasing energy barrier is predicted to cause the tethering rate to diminish with the natural logarithm of time. Theory also predicts that the tethered chains must stretch away from the solid surface to avoid each other as the number of tethered chains per unit of surface area increases. The second regime is predicted to end when the chains become so stretched due to crowding that further tethering is energetically unfavorable, i.e., when the entropy cost associated with tethering balances the energy benefit associated with formation of the chemical bond between the polymer chain and the solid surface. The cessation of tethering is called saturation.

Two points in the above-described tethering process are notable, and they are illustrated in Figure 1. One of these is the end of the first regime (beginning of the second regime), where the chains are on the verge of overlapping, but are still in the relaxed configuration; here they are depicted as hemispherical coils, called mushrooms (Figure 1a). The other, of course, is saturation, where the chains are in a stretched configuration, called collectively a brush (Figure 1b). Because our earliest experiments gave indications that the tethering process differed qualitatively from that described above, we were particularly interested in making a comparison of the kinetics predicted by theory with the kinetics obtained experimentally.

10.1021/ma020618o CCC: $22.00
Published on Web 07/27/2002

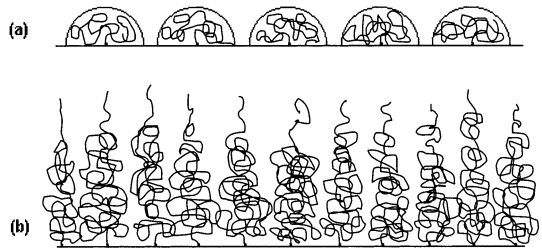

Figure 1. Drawings of tethered layer conformations as predicted by theory. (a) The mushroom layer consists of nonoverlapping, coiled tethered chains, and (b) the brush layer consists of crowded, stretched tethered chains.

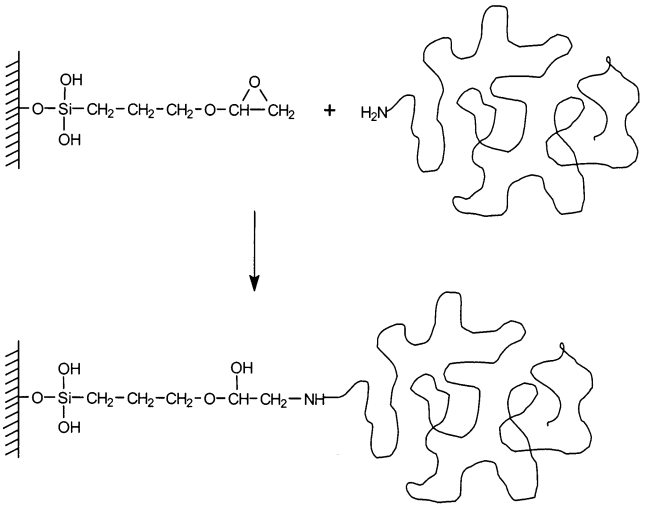

Figure 2. Schematic diagram of chemical reaction between functional end group on polymer chain and active site on surface of the substrate. This is the chemical reaction by which polymer chains are tethered to the solid surface.

Our approach to studying the kinetics of layer formation was to place a solid substrate in contact with a stirring solution of polymer and to monitor the disappearance of polymer from solution with time. The polymers used for tethering were monodisperse polystyrene chains, terminated at one end with a primary amine functional group. The impenetrable solid used as a substrate was silicate glass, the surface of which had been treated previously to contain epoxide functional groups, which are known to react readily with primary amine groups. Figure 2 shows the chemical reaction responsible for tethering. The disappearance of polymer from solution was monitored by means of a pseudo-real-time, off-line method based on size exclusion chromatography.[20] This method was made quantitative by use of an internal standard, and the absence of interference from polymer adsorption was confirmed by means of auxiliary experiments.

II. Experimental Section

A. Synthesis and Characterization of Amine Functional-Ended Polystyrene. Benzene and styrene were purified as described previously.[21] Lithium chloride (Fisher, 99.8%) was used as received, except for drying in the polymerization reactor at 150°C on the vacuum line for 1 h. *N*-3-Chloropropyl-2,2,5,5-tetramethyl-2,5-disila-1-azacylopentane (FMC, Lithium Division, Research Grade) was stirred over calcium hydride and distilled into calibrated ampules followed by dilution with benzene. *sec*-Butyllithium (FMC, Lithium Division, 12 wt % in cyclohexane) was used as received and was titrated by the Gilman double titration method with 1,2-dibromoethane.[22] *N*-Trimethylsilyldiphenylcarbimide was prepared from sodium bis(trimethylsilyl)amide (Aldrich, 99%) and benzophenone as described by Kruger et al.[23] The resulting carbimide was stirred over calcium hydride and distilled into calibrated ampules.

Polymerization and functionalization reactions were carried by means of standard high-vacuum techniques in sealed, all-glass reactors equipped with break-seals.[24] ω-(3-Aminopropyl)-polystyrene was prepared as follows. Lithium chloride (7.5 mmol) was added to the polymerization reactor and was heated at 150°C for 1 h at reduced pressure. After *sec*-butyllithium (3.5 mmol) was injected into the reactor, benzene (150 mL) was distilled in, and then styrene (13.9 g) was added by breaking the break-seal on the corresponding ampule. After 6 h at room temperature, the solution was transferred into several ampules, including one that contained a small sample of base polymer (terminated with methanol). A benzene solution of *N*-3-chloropropyl-2,2,5,5-tetramethyl-2,5-disila-1-azacyclopentane (4.22 mmol) was added to the poly(styryl)-lithium solution (2.81 mmol). After 6 h, the mixture was quenched by addition of degassed methanol. The polymer was isolated by precipitation into excess methanol. For polystyrene of low molecular weight, deprotection was accomplished by multiple reprecipitation into methanol, with completeness of deprotection monitored by proton NMR. Because monitoring by NMR was problematic for the high-molecular-weight polystyrene, the 44 K protected polymer (ω-*N*-1,1,4,4-tetramethyldisilylazacyclopentanepolystyrene) was converted to the corresponding primary amine by reduction with $NaBH_4$ as follows.[25] After 10.5 g of protected polymer (0.26 mmol) was dissolved in 120 mL of a 50/50 tetrahydrofuran/ethanol solution, $NaBH_4$ (2.6 mmol, 0.098 g) was added, and the mixture was heated under reflux for 3 h. The excess $NaBH_4$ was quenched by slow addition of 0.5 mL of deionized water. The primary amine functional-ended polymer was recovered by precipitation into methanol. Any nonfunctionalized, polymeric dimer was separated from the desired product by sequential elution with toluene and THF though a silica gel column.

Molecular weight and molecular weight dispersity of the purified polymer were characterized by means of size exclusion chromatography (SEC) at a flow rate of 1.0 mL/min in tetrahydrofuran (THF) at 30 °C with a Waters 150C-Plus system equipped with six UltraStyragel columns (500, 2×10^3, 10^4, 10^5. and 10^6 Å), a Waters differential refractometer and a Viscotek viscosity detector after calibration with polystyrene standards from Polymer Laboratories. Four polymer molecular weights were prepared for this study: M_n = 4000, 15 000, 20 000, and 44 000. In all cases, dispersity, M_w/M_n, was <1.04, and the primary amine end group was $-(-CH_2-)_3NH_2$. The fraction of chains containing primary amine end groups was determined by titration in 1/1 (v/v) mixture of chloroform in glacial acetic acid with perchloric acid (Fisher, 10.1 N in glacial acetic acid) as the titrant and methyl violet 2B (Aldrich, about 75% dye content) as the indicator;[26] five to seven 0.5-g samples were analyzed from each batch of polymer. End-functionalization was found to be >95% for all batches of polymer.

B. Introduction of Active Sites to Surface of Silicate Glass Substrate. Silicate glass in the form of spherical beads (Grade 500 UNC, Lot #0600R1948) was procured from Potters Industries, Cleveland, OH, for use as the solid substrate. According to the manufacturer, the beads had a mean diameter of 10 μm, a specific surface area of 0.24 m^2/g, and no surface treatment. Before use, beads were cleaned as follows to remove contamination and expose the native hydroxyls. One hundred grams of as-received glass beads were placed in a beaker and were covered with piranha solution (70 mL of H_2SO_4 and 30 mL of 30% aqueous H_2O_2). This slurry was heated for 2 h at 90 °C with vigorous stirring. After heating and stirring were stopped, the mixture was allowed to settle and the acidic liquid was decanted. The beads were washed repeatedly with water until the decanted rinse water reached a pH of 7.0. The neutral slurry was filtered with the aid of vacuum through an alumina filter membrane containing 0.02-μm pores (Anodisc 47, Whatman Int., Maidstone, England). On the filter membrane, the beads were washed with acetone three times to remove water and were dried in a vacuum oven at 110 °C for 24 h. One batch

of cleaned beads was subjected to scanning electron microscopy for verification of the diameter and surface area values provided by the manufacturer.

Functional groups were introduced to the surface of the glass by derivatization of the native hydroxyl groups with 3-glycidoxypropyltrimethoxysilane (98%, Aldrich, Minneapolis, MN). This treatment linked epoxide groups to the underlying glass surface by flexible, six-atom spacer arms (see Figure 2). The procedure was based on similar procedures developed for functionali-zation of silicate glass substrates used as chromatography supports, e.g., refs 27−29 Fifty grams of clean, dry glass beads and 100 mL of toluene (reagent grade) were placed in a 250 mL, round-bottomed flask fitted with a condenser. Then 2.5 mL of 3-glycidoxypropyltrimethoxysilane were added with a syringe, and the mixture was stirred at reflux for 24 h. The cooled mixture was filtered on an Anodisc 47 filter membrane (see above), and the beads were rinsed several times with toluene while still on the filter. The beads were then subjected to Soxhlet extraction for 48 h with toluene (about 96 extraction cycles) to remove any silane reagent that was not chemically bonded to the surface. The beads were dried under vacuum at 110 °C for 24 h and were stored in a desiccator until needed. The presence of 3-glycidoxypropylsilyl groups chemically bonded to the glass surface was confirmed by treating the beads with TBAF reagent (tetrabutylammonium fluoride, 1.0 M in THF from Aldrich, Milwaukee, WI), which is known to specifically cleave the −Si−O− bond, followed by analyzing the cleavage medium by means of gas chromatography−mass spectrometry. The mass spectrum obtained was compared with the mass spectrum of pure 3-glycidoxypropyltrimethoxysilane that had been exposed to TBAF. The peak-for-peak equivalence of the spectra indicated that the species cleaved from the glass surface was indeed the 3-glycidoxypropylsilyl group. Dye coupling analysis[30,31] conducted previously[32] showed that beads treated in this way have a mean value of 2.71 ± 0.24 epoxide groups/nm^2.

C. Setup of the Tethering Reaction. At the beginning of this work, we used tetrahydrofuran as a solvent for the tethering reactions. Because of the high scatter, mainly due to the buildup of peroxides in the lengthy reactions, we switched to toluene as a solvent. The tethering reactions run in toluene were always done as twins, i.e., as duplicate reactions run at the same time with epoxidized beads from the same batch and with polymer solution that had been freshly made up in a larger quantity and divided in half. The amounts and procedures given below pertain to a single reaction. All glassware used in tethering reactions was exposed to *n*-butyl-trichlorosilane reagent to prevent segmental adsorption of polystyrene. The three necks of a 100 mL, round-bottomed flask were fitted with a condenser, an argon inlet, and a glass stopper, respectively. Teflon sleeves were used to seal all ground glass joints. Under a slight positive pressure of argon, the flask was charged with 20 mL of reagent grade toluene (or THF) into which had been dissolved 0.0051 g of functional-ended polystyrene and 0.0020 g of internal standard. The internal standard used was monodisperse polystyrene (Polysciences, Inc., Warrington, PA), inert-ended so it could not take part in the tethering reaction. The molecular weight of the internal standard was always chosen so its elution peak in size exclusion chromatography would not overlap that of the functional-ended polystyrene. Then 18.1 g of epoxidized glass beads were added, and the resulting slurry was stirred at low speed during the reaction to keep the beads from settling.

The above ratio of 0.0051 of functional-ended polymer to 18.1 g of epoxidized glass beads was used in all experiments except $M_n = 4000$ in THF, for which the ratio was 0.0073 g of polymer to 6.0 g of beads. Both ratios provided an excess of epoxide sites over functional-ended polymer chains, so that the amount tethered was not limited by the number of active sites on the substrate.

D. Monitoring of Tethering Reaction. Aliquots of approximately 0.5 mL were withdrawn periodically from the stirring reaction mixture with polypropylene transfer pipets (Fisher Scientific, Pittsburgh, PA). Since each aliquot contained both glass beads and polymer solution, the ratio of beads to liquid in the reaction flask remained constant although the amount of mixture diminished incrementally with each aliquot taken. The aliquot was inserted into the barrel of a syringe that had been previously treated with *n*-butytrichlorosilane and was pushed through a syringe filter (Scientific Resources, Eatontown, NJ) of 0.54 μm pore size to separate the beads from the polymer solution. The beads were discarded, and 50 μL of bead-free filtrate was injected into a liquid chromatograph for analysis by size exclusion chromatography (SEC). The chromatograph (Waters Corp., Milford, MA) was equipped with two Waters Styragel columns (HR1 and HR3) and a UV detector. Columns were eluted at a flow rate of 1 mL/min with HPLC-grade THF as the mobile phase. Data from the chromatograph were acquired by computer and were reduced with the aid of DAx 7.0 data acquisition and handling software (van Mierlo Software, Eindhoven, The Netherlands). Mass of functional-ended polymer in the solution phase of the aliquot was determined from area under its elution peak. Because of the possibility of evaporation of small amounts of solvent during handling of the aliquot, this peak was always checked and corrected if necessary with reference to the peak of the internal standard. Peak area at each time sampling time, t, was normalized by peak area at $t = 0$ (before addition of beads) to yield mass fraction of functional-ended polymer in solution. Mass tethered at any given sampling time, *t*, was taken to be equal to mass disappeared from solution since $t = 0$.

E. Auxiliary Experiments to Check for Segmental Adsorption. We sought to do tethering experiments that were not confounded by the occurrence of segmental adsorption of either functional-ended polystyrene or the inert-ended internal standard on the epoxidized beads. The possibility of segmental adsorption was evaluated by means of auxiliary experiments with *inert-ended* polystyrene, for which tethering was not possible. The first auxiliary experiment involved exposing epoxidized glass beads to a solution of *two* inert-ended, monodisperse polystyrene standards ($M_n = 2300$ and $M_n = 46\,000$) under the same conditions used for tethering reactions, monitoring the mixture by means of SEC as described above. Were adsorption to occur, it would be expected to exhibit the well-known pattern of preferential adsorption of the higher molecular weight species at long times,[33] and a change in the peak ratio in successive chromatograms would be expected to develop. In the absence of adsorption, the peak ratio in successive chromatograms would be expected to remain constant. The second auxiliary experiment consisted of exposing epoxidized glass coverslips to *inert-ended* polystyrene ($M_n = 40\,000$) under the conditions used for tethering reactions, extracting the slips in a Soxhlet apparatus and examining them for adsorbed polystyrene by means of contact angle measurements and atomic force microscopy. (While X-ray photoelectron spectroscopy might seem to be a suitable surface analysis method, neither its surface sensitivity nor its quantitative accuracy is sufficient to be of benefit in these studies.)

F. Atomic Force Microscopy. Atomic force microscopy (AFM) was conducted in the contact mode with a JEOL JSPM 4200 atomic force microscope (Japan Electron Optics). Specimens were examined in air with a silicon nitride tip. AFM was conducted in the tapping mode with a Digital Instruments model MMAFM-110EX Nanoscope (Santa Barbara, CA) multimode atomic force microscope. Specimens were examined in air with a model ESP contact-etched silicon probe. Test surfaces were prepared on glass coverslips (Fisherbrand, Fisher Scientific, Pittsburgh, PA) because the flat geometry was convenient for positioning in the AFM. Mushroom and brush layers were tethered to the coverslips under reaction conditions exactly the same as those used for glass beads. However, after the coverslips were removed from the tethering medium and drained of solvent, they were subjected to extraction in a Soxhlet to remove any nontethered chains that might have merely deposited during draining.

G. Scanning Electron Microscopy. Scanning electron microscopy (SEM) was conducted on a Hitachi S3200 variable pressure SEM (Hitachi). Application of conductive coatings to

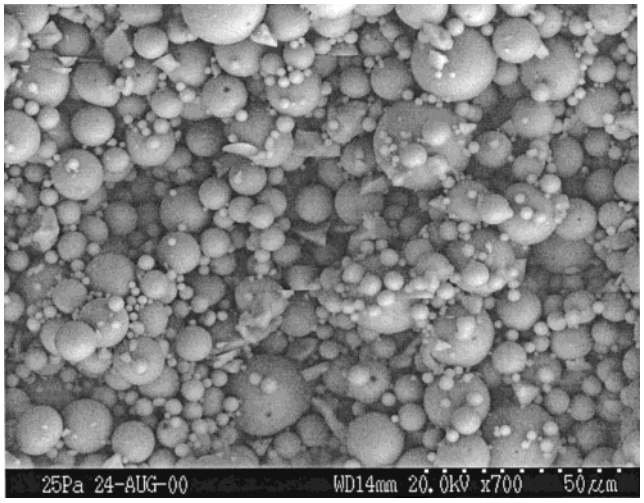

Figure 3. Scanning electron micrograph of glass beads at a magnification of 700×. Note the smooth, nonporous surfaces.

the specimens was unnecessary, since the chamber was operated at a pressure of 25 Pa rather than at full vacuum. Images were obtained at 20.0 kV.

III. Results and Discussion

A. Substrate Surface Area. Scanning electron microscopy performed on a sample of beads after they were treated with piranha solution showed them to be smoothed-surfaced and spherical (Figure 3). From a micrograph at a magnification of 700×, the diameters of 200 beads selected at random were measured, and the surface area was computed for each bead. The mean surface area was 0.24 m^2/g, in good agreement with the value provided by the manufacturer.

B. Absence of Segmental Adsorption. The auxiliary experiments done to check for segmental adsorption showed complete absence of adsorption. First, the two constituents of the low and high molecular weight, *inert-ended* polystyrene exposed to epoxidized glass beads showed no change in absolute or relative amount over time (150 h), other than random experimental variation of less than 2%. Second, the AFM images of epoxidized coverslips before and after exposure to *inert-ended* polystyrene (M_n = 40 000) were indistinguishable, as shown by Figure 4, parts a and b, and were typical of smooth glass surfaces treated with organofunctional silane reagents.[34] Similarly, contact angle measurements indicated absence of segmental adsorption onto the epoxidized surfaces. Contact angles are not only very surface-sensitive (sensing only the top 0.5 nm) but also very sensitive to changes in surface chemistry. This is shown by the data in Table 1, where it can be seen that the low contact angle of pristine glass was increased considerably by exposure to laboratory air, which contained adventitious hydrocarbons. The glass surface to which polystyrene chains were tethered gave a contact

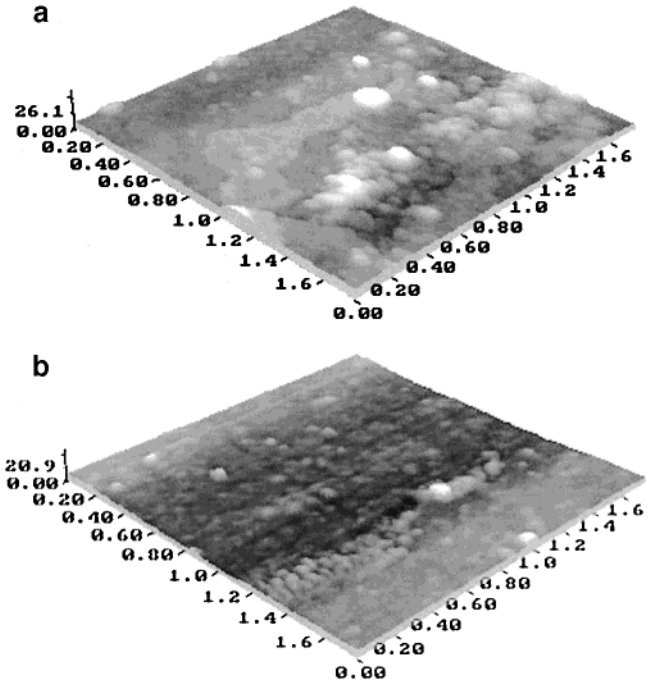

Figure 4. Atomic force microscope images of glass coverslips having epoxidized surfaces: (a) before exposure to solution of inert-ended polystyrene and (b) after exposure to solution of inert-ended polystyrene. The images were obtained in contact mode in air. The horizontal scale is in micrometers, and the vertical scale at the left-hand corner of each image is in nanometers.

angle typical of commercial polystyrene, while the epoxidized surface gave a significantly lower contact angle. After exposure to inert-ended polystyrene, the contact angle of water on the epoxidized surface remained the statistically indistinguishable from before, consistent with total absence of any polymer on the surface.

C. Tethering Kinetics. In the present work, tethering reactions were conducted from dilute solution and were of long duration. Our experiments did not escape the difficulties typically associated with lengthy experiments; instrument instabilities and overnight equipment failures resulted in numerous invalidations or total losses of experiments. In addition, the synthesis of the functional-ended polymer was done on a relatively small scale, so that when one particular molecular weight was consumed, a different molecular weight had to be used. Hence, it was not possible to use exactly the same array of molecular weights for all solvents, temperatures, etc.

The results of tethering reactions under various conditions are shown in Figures 5−12, which present polymer left in solution vs time. Note the switch from linear to log time on the *x*-axis in each figure. The initial, or zero time, point for each tethering reaction was the

Table 1. Contact Angles Made by Water on Modified and Nonmodified Glass Surfaces

treatment	contact angle, deg[a]
pristine: washed in acid, rinsed, blow-dried, and subjected to immediate contact angle measurement	0
washed and aired: washed in acid, rinsed, dried in a vacuum and exposed to ambient air	21 ± 2.8
epoxidized: derivatized with glycidoxy-propyltrimethoxysilane under anhydrous conditions	54 ± 3.7
exposed: epoxidized and exposed to inert-ended polystyrene of M_n = 40 000	57 ± 4.0
polystyrene-tethered: epoxidized and reacted with primary-amine-ended, monodisperse polystyrene of M_n = 44 000	83 ± 4.6

[a] Mean of at least six values, ±1 std dev.

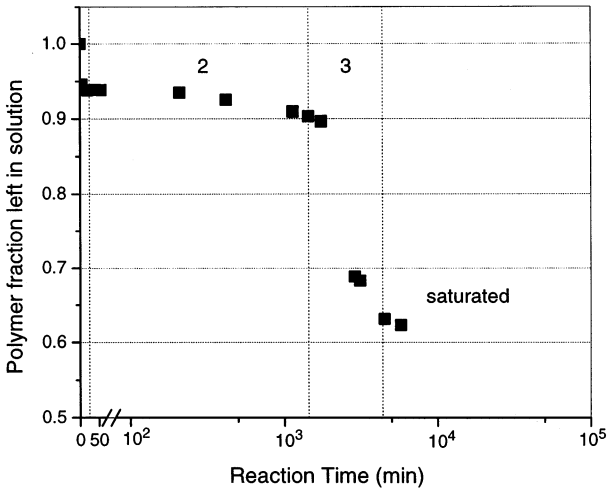

Figure 5. Plot of polymer fraction left in solution vs reaction time for functional-ended polystyrene of $M_n = 4000$ at 60 °C in THF. Vertical lines separate the regimes. The second and third regimes are identified by large numbers 2 and 3.

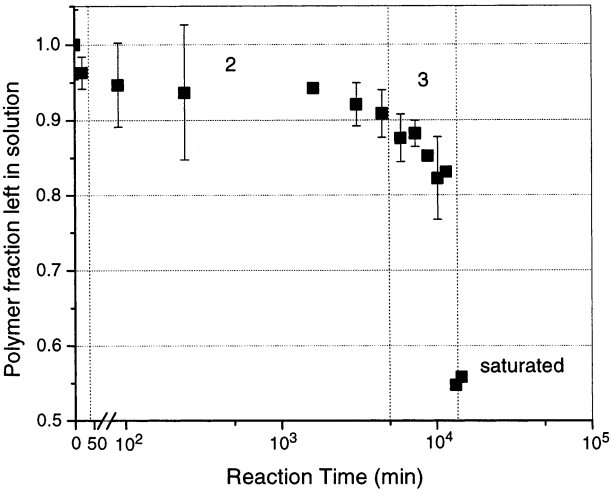

Figure 6. Plot of polymer fraction left in solution vs reaction time for functional-ended polystyrene of $M_n = 20\,000$ at 60 °C in THF.

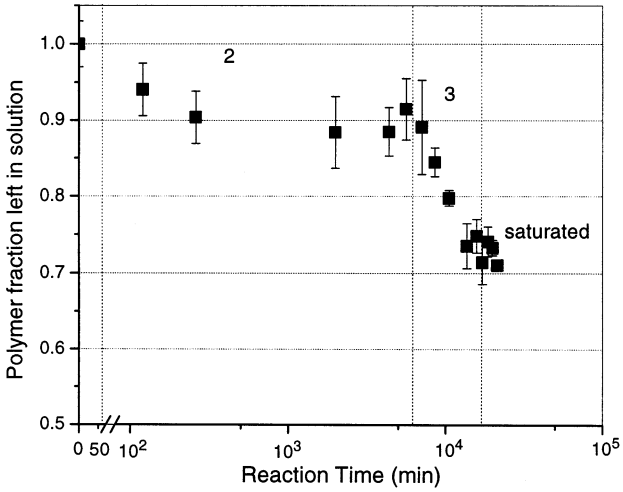

Figure 7. Plot of polymer fraction left in solution vs reaction time for functional-ended polystyrene of $M_n = 44\,000$ at 60 °C in THF.

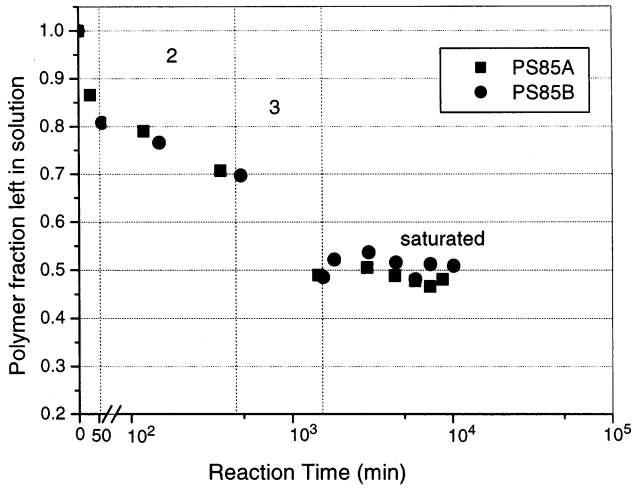

Figure 8. Plot of polymer fraction left in solution vs reaction time for functional-ended polystyrene of $M_n = 15\,000$ at room temperature in toluene.

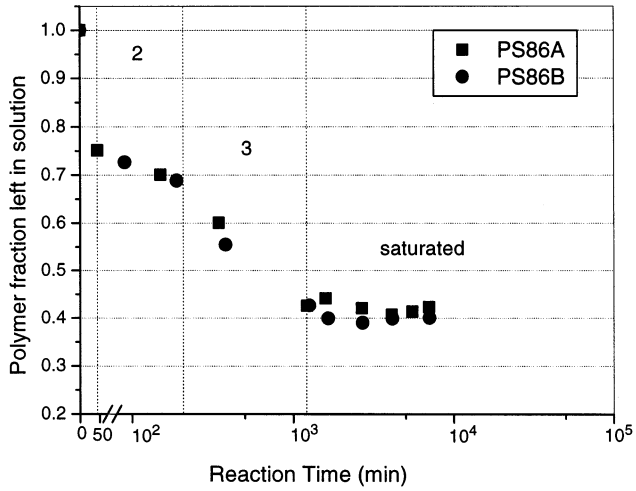

Figure 9. Plot of Polymer fraction left in solution vs reaction time for functional-ended polystyrene of $M_n = 15\,000$ at room temperature in toluene. This duplicates reactions in Figure 8.

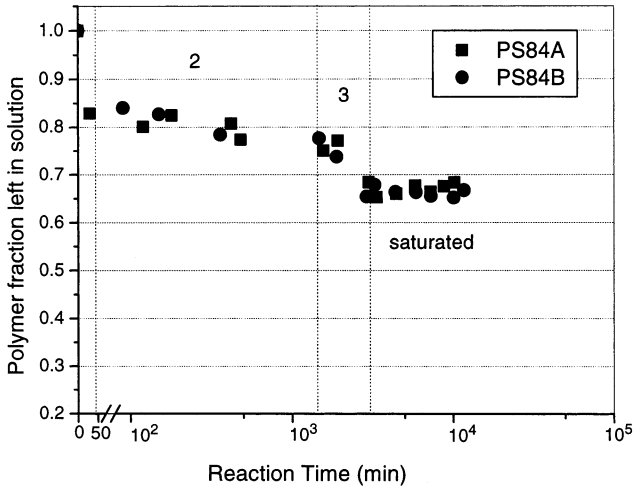

Figure 10. Plot of polymer fraction left in solution vs reaction time for functional-ended polystyrene of $M_n = 44\,000$ at room temperature in toluene.

mean of three to four replicate aliquots taken just before addition of the epoxidized beads; the scatter about this mean was always less than the size of the symbol used to represent the initial point. For the tethering reactions run in THF (Figures 5−7), points taken after the initial one showed quite a lot of scatter. We attribute much of

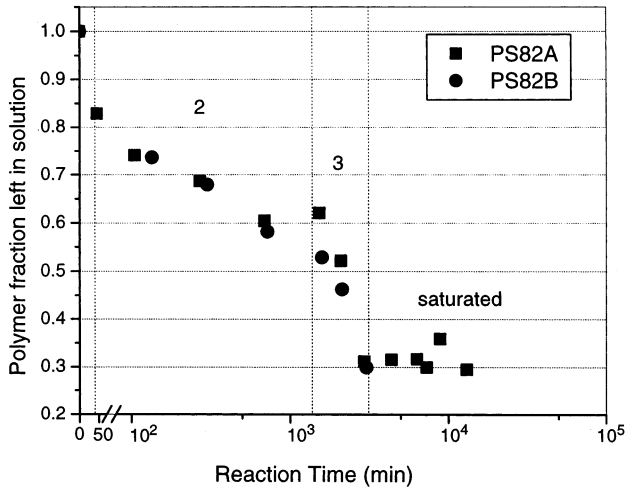

Figure 11. Plot of polymer fraction left in solution vs reaction time for functional-ended polystyrene of M_n = 15 000 at 100 °C in toluene.

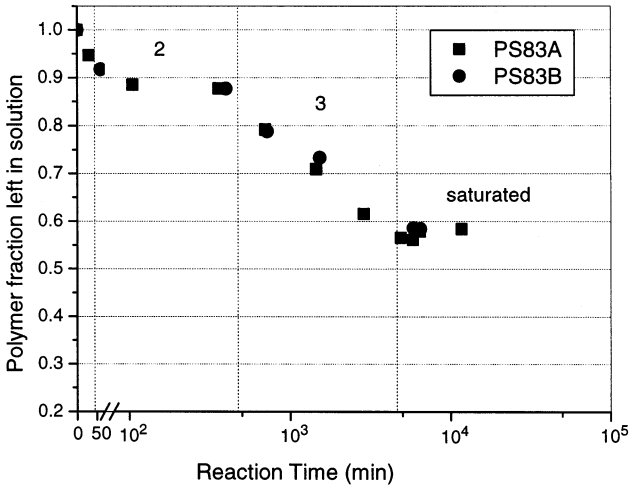

Figure 12. Plot of polymer fraction left in solution vs reaction time for functional-ended polystyrene of M_n = 44 000 at 100 °C in toluene.

this scatter to the buildup of peroxides, a well-known problem for ethereal solvents. Points without error bars in Figures 5−7 represent values for single aliquots, and those with error bars represent the mean of three aliquots taken within an hour of each other. The scatter associated with the use of THF as a solvent prompted us to switch to toluene after we had collected the data shown in Figures 5−7.

Results of the tethering reactions run in toluene at room temperature are shown in Figures 8−10. As described in the Experimental Section, reactions in toluene were run as twins, i.e., duplicate reactions run and monitored side by side. Data from the two members of each set of twins are represented by two different symbols on the same plot. The initial point in each plot was determined as described above, and each data point after the initial represents the value obtained from a single aliquot withdrawn from the reaction. Figures 8 and 9 show results for M_n = 15 000 at room temperature, while Figure 10 is for M_n = 44 000 at room temperature. Figures 11 and 12 present results of tethering reactions done at elevated temperature (100 °C) in toluene. In each figure of the series in Figures 8−12, the two members of each set of twins show very good reproducibility, while Figures 8 and 9 show the fairly good reproducibility achieved by two sets of twins under the same reaction conditions.

The most interesting thing by far in Figures 5−12 is the appearance of three regimes of kinetics prior to saturation instead of the two regimes predicted by theory. Despite the scatter in Figures 5−7, three regimes of kinetics can be discerned. Figures 8-12 show the three regimes even more clearly. In each figure, dotted vertical lines have been inserted to separate one regime from the next. The first regime is one of rapid tethering, in which approximately 10 mass % of the polymer in solution is tethered within 1 h. The second regime is characterized by an extremely slow tethering rate, requiring a change in the scale of the *x*-axis from time to log(time). Tethering in the second regime appears to be proportional to log(time). The third, and unpredicted, regime is characterized by accelerated tethering. Tethering in the third regime also appears to be proportional to log(time), but with a steeper slope. The third regime ends when saturation is reached. Although data were collected beyond the time of saturation to verify that saturation had been reached, multiple data points collected after saturation do not constitute a fourth regime. Each regime is discussed in more detail below.

The first regime, according to theory, is one in which the kinetics of tethering is controlled by center-of-mass diffusion of the polymer chains through the solvent to the surface. (Diffusion of the functional end of the chain to an active site on the surface is fast by comparison.) Recall that the reactions in this study were stirred just fast enough to keep the beads from settling. In this case, the laminar flow generated around each bead produces a pseudo-steady state concentration gradient between the bulk solution and the nonmoving boundary layer attached to the surface of each bead. Center-of-mass diffusion of polymer chains through a boundary layer that sustains only diffusion and no convection would correspond to a rate proportional to time. (This is unlike quiescent systems, in which control by center-of-mass diffusion corresponds to a rate that is proportional to $\sqrt{\text{time}}$.) We could not make sufficient numbers of measurements within this short-lived first regime to fully characterize its time dependence. Therefore, we cannot authoritatively claim that the tethering rate is proportional to time, although our data are not inconsistent with such a claim.

Verification that the end of the first regime corresponded to completion of a mushroom layer was made by confirming that the mass tethered was equivalent to the mass of a layer of relaxed polymer coils on the verge of overlap. This was done by comparing experimentally determined surface attachment densities and chain radii with the same quantities computed from theory. Experimental surface attachment densities were computed from (mass tethered × Avogadro's number) ÷ (molecular weight × total surface area). Mass tethered for each reaction was taken to be the fraction of polymer that had disappeared from solution multiplied by the initial mass of polymer. Initial mass was 0.0051 g and total surface area was 4.34×10^{18} nm^2 in all cases, except for M_n = 4000 in THF, where the amounts differed slightly as noted in the Experimental Section. Surface attachment density was converted to a corresponding equivalent radius, $R_e = [\pi(\text{chains/nm}^2)]^{-1/2}$, which is a measure of the surface area associated with a single tethered chain. R_e is to be compared with the

Table 2. Characteristics of Layers Formed in THF at 60 °C

mol wt, M_n	fraction tethered[a−c]	chains/nm^2, from data	radius, R_e (nm) from data	radius, R_g (nm) from theory	chains/nm^2 from $(\pi R_g^2)^{-1}$
4000	0.05 (M)	0.038[d]	2.9	1.7	0.11
4000	0.40 (B)	0.30	1.0	1.7	N.A.
20 000	0.05 (M)	0.0018	13.4	6.4	0.0078
20 000	0.45 (B)	0.016	4.5	6.4	N.A.
44 000	0.10 (M)	0.0016	14.1	10.3	0.0030
44 000	0.30 (B)	0.0048	8.1	10.3	N.A.

[a] Fraction disappeared from solution. [b] M indicates completed mushroom layer. [c] B indicates completed brush, i.e., at saturation. [d] Amounts of beads and polymer used for this reaction were slightly different than for other molecular weights.

Table 3. Characteristics of Layers Formed in Toluene at 23 °C

mol wt, M_n	fraction tethered[a−c]	chains/nm^2, from data	radius, R_e (nm) from data	radius, R_g (nm) from theory	chains/nm^2 from $(\pi R_g^2)^{-1}$
15 000	0.20 (M)	0.0094	5.8	5.4	0.011
15 000	0.50 (B)	0.024	3.7	5.4	N.A.
44 000	0.15 (M)	0.0024	11.5	10.3	0.0030
44 000	0.35 (B)	0.0056	7.5	10.3	N.A.

[a] Fraction disappeared from solution. [b] M indicates completed mushroom layer. [c] B indicates completed brush, i.e., at saturation.

Table 4. Characteristics of Layers Formed in Toluene at 100 °C

mol wt, M_n	fraction tethered[a−c]	chains/nm^2, from data	radius, R_e (nm) from data	radius, R_g (nm) from theory	chains/nm^2 from $(\pi R_g^2)^{-1}$
15 000	0.20 (M)	0.0094	5.8	5.4	0.011
15 000	0.70 (B)	0.033	3.1	5.4	N.A.
44 000	0.10 (M)	0.0016	14.1	10.3	0.0030
44 000	0.40 (B)	0.0064	7.0	10.3	N.A.

[a] Fraction disappeared from solution. [b] M indicates completed mushroom layer. [c] B indicates completed brush, i.e., at saturation.

radius of gyration of a relaxed polymer coil in a good solvent,[35] $R_g = (1/\sqrt{6})N^{3/5}a$, where N is the degree of polymerization and a is the statistical segment length, which is taken to be 0.67 nm for polystyrene.[36] (For $M_n = 4000$, $R_g = (1/\sqrt{6})N^{1/2}a$ was used, which better represents chains with $N \leq 40$.[37]) Theoretical surface attachment densities for each molecular weight were computed from $(\pi R_g^2)^{-1}$. The experimental and theoretical values are presented in Tables 2−4, where rows pertaining to the end of the first regime, are indicated by M, for mushroom. For a mushroom layer, R_e is expected to be at least as large as R_g, and this is what is found in every case, no matter what temperature and solvent were used. Correspondingly, the experimentally determined surface attachment density is slightly lower than that of a hypothetical layer of mushrooms, or hemispherical caps, with radii equal to R_g. A closer comparison of R_e with R_g reveals that there is not quite enough space between relaxed chains, or mushrooms, on the experimental surface to accommodate an additional relaxed chain of radius R_g. From this, we can conclude that the end of the first regime coincides with a layer of loosely packed and relaxed chains, i.e., mushrooms.

The second regime in Figures 5−12 seems to agree with theory, in that tethering appears to be proportional to log(time), as expected for an energy barrier to polymer diffusion that progressively increases with an increasingly crowded tethered layer.[13,14] It should be noted that the surface attachment density increases relatively little during the second regime.

The third regime in Figures 5−12 is defined by an accelerated rate of tethering. This behavior, termed by us "layer-assisted tethering",[8] is not predicted by existing theory. Because tethering in this regime, as in the second, also appears to follow a log(time) relation, the notion of a progressively increasing energy barrier again must be invoked. However, to account for the increase in tethering rate with respect to the second regime, the progressive increases in the energy barrier with increasing densification of the layer must be assumed to be smaller than in the second regime. We can speculate why the energy barrier would increase more slowly at a later stage in tethering. It has already been suggested that free chains, diffusing into the tethered layer, might contract laterally to fit into small spaces on the surface between already-tethered chains.[38] We speculate that, in addition to this, the *already-tethered* chains also contract laterally (and simultaneously stretch vertically) when perturbed by an incoming chain. Lateral contraction by the already-tethered chains not only would make room for the incoming chain, but also would generate space on the sides away from the incoming chain—space that could be exploited by subsequent incoming chains. The extra space opened in response to just a few incoming chains in a small area could be considerable and could possibly lead to an avalanche of tethering. We will discuss this speculation later in conjunction with a model of the tethering process.

The end of the tethering process, saturation, can be discussed in terms of the same quantities used for the mushroom layer. Tables 2−4 present these values in rows indicated by B, for brush. At saturation, R_e is less than R_g in every case, which suggests that the chains in the saturated layer are compressed laterally relative to their relaxed states. This is consistent with the notion of a brush, i.e., chains that are laterally compressed, and therefore stretched away from the surface. For all of the tethering reactions, the surface attachment densities at saturation are more than double those found at the end of the first regime (mushroom layer). It should be noted that the surface attachment densities at saturation are much less than 2.71/nm^2, the area density of active sites on the glass substrate prior to tethering. This means that the density of active sites was more than sufficient to accommodate the surface attachment density reached by the tethered chains. Nevertheless, compared with the very dense brushes that can be made by surface-initiated grafting,[39] the brushes formed in the present study qualify as only moderately dense.

As for the effect of experimental variables on the final tethered layers, some general observations can be made. First, as fully expected, the surface attachment density (chains/nm^2) declined as molecular weight increased. A log−log plot of molecular weight vs surface attachment density (chains/nm^2) forms the straight line shown in Figure 13. Second, elevation of the temperature, with solvent held constant, resulted in an increase in amount tethered. Although this temperature effect is not very noticeable in the log−log plot of Figure 13, it is quite clear from the values in Tables 3 and 4. Third and finally, the amount tethered from THF was lower than

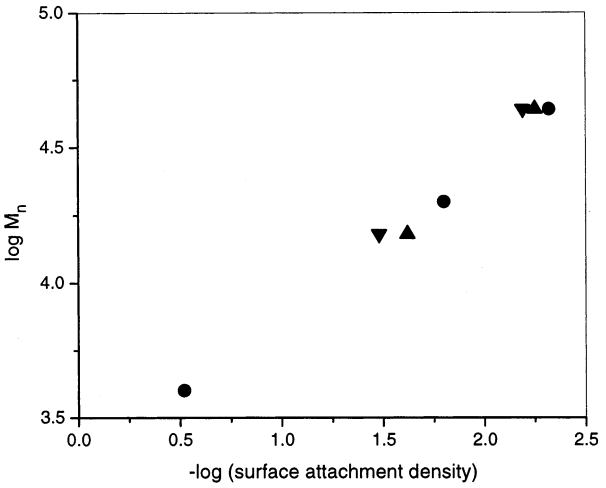

Figure 13. Plot of log of molecular weight (M_n) vs negative log of surface attachment density (chains/nm^2).

from toluene. This can be deduced from Tables 2 and 3, where reactions in THF at 60 °C are compared with those in toluene at room temperature, and molecular weights of 15 000 and 20 000 are assumed similar enough to be comparable.

D. A Model. We sought to develop a mathematical or statistical model that would not only predict three dis-tinct regimes but also would support the idea of "layer-assisted tethering", described above as an explanation for what was observed experimentally. Tethering, like polymer adsorption, can be regarded as a deposition process, and many deposition processes have been modeled as random sequential adsorption (RSA), in which the sites on the surface are chosen randomly and are filled irreversibly. When the RSA model is generalized to include interaction between the depositing species, it is more appropriately called cooperative sequential adsorption (CSA). Various versions of random and cooperative sequential adsorption of many different types of objects have been developed.[40−42]

In the actual physical situation, the tethered layer corresponds to a relatively sparse layer of chains in the relaxed (mushroom) configuration at an early stage and ends as a more densely packed layer of chains, stretched away from the surface (brush). We also know that only the reactive end of each chain, and none of the segments within it, is affixed to the surface. Therefore, we can reason that the already-tethered chains in the mushroom configuration can be laterally compressed (either by their neighbors or by incoming chains) in order to reach the brush state. Self-consistent-field methods[43] and molecular dynamics simulations[44] have shown that chains tethered by one end to a solid substrate in the presence of solvent do not stretch uniformly away from the substrate. Instead, the monomer density is a parabolic function of distance from the substrate. Thus, close to the substrate, the monomer volume fraction would approximate that of a semidilute solution, but in the outer reaches of the tethered layer, away from the substrate, the monomer volume fraction would be closer to that of the bulk solution, which is dilute (see Figure 1). In these circumstances, free chains should be able to diffuse into the outer reaches of the tethered layer fairly easily, almost as to a bare surface, but would encounter increasing resistance as they moved through the denser part of the tethered layer toward the solid surface itself. Dynamic Monte Carlo simulations of the

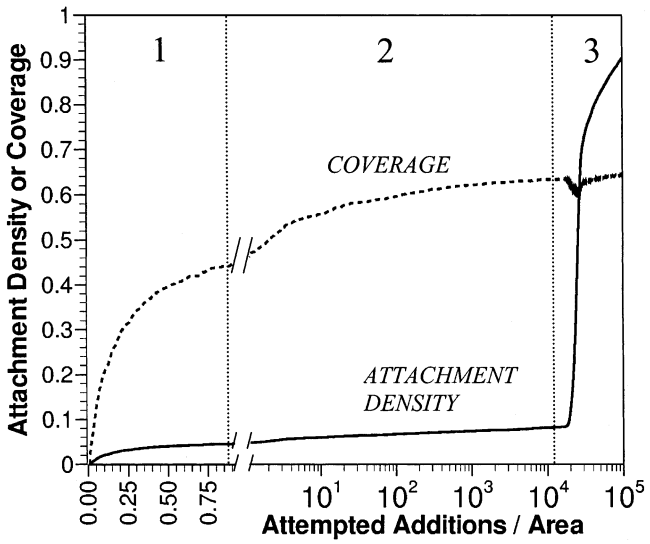

Figure 14. Plot of normalized surface attachment density and fractional coverage by tethered disks vs log of number of MC tethering attempts per unit area. The thin vertical lines illustrate that the simulations follow the expected behavior in all three kinetic regimes.

tethering of individual self-avoiding chains have shown behavior consistent with these ideas and have suggested that the tethering of an individual, incoming chain starts with spontaneous lateral contraction of the chain due to thermal fluctuations.[45]

With these considerations in mind, we planned a Monte Carlo simulation of a CSA process in which a polymer chain was represented by a disk that could not overlap other disks and that maintained a circular cross-section parallel to the surface of the substrate. Each step of the simulation consisted of an attempt to add one disk irreversibly to a randomly selected location on a fixed area of flat surface. All disks were assumed to have the same radius, R_g, in the relaxed state, but both the already-tethered disks and the incoming disks could undergo lateral contraction.

In our simulation, the overall probability of adding a disk at the selected location and within the time interval of a Monte Carlo step depended on two particular probabilities. The first was expressed as $e^{-E_{diff}A_O/kT}$, in which E_{diff} was an energy barrier analogous to that for center-of-mass diffusion of a free polymer through semidilute solution, i.e., through the denser part of the tethered layer closer to the substrate. It was an adjustable parameter in the simulation, made dimensionless by division by kT. A_O was the fractional area of overlap between the incoming disk of radius R_g and all previously tethered disks. It ran from zero to one and was analogous to the local crowding experienced by a polymer chain. This probability could run from one to $e^{-E_{diff}/kT}$, as the surface ran from bare ($A_O = 0$) to completely filled ($A_O = 1$). In the simulation, a disk was allowed to proceed to the surface if a random number chosen uniformly from the interval [0,1] was less than $e^{-E_{diff}A_O/kT}$. A similar approach was taken by Zhdanov and Dasemo to model the energy barrier produced by a growing layer of deformable proteins.[46]

The second particular probability was expressed as $e^{-\Delta F_{def}/kT}$, in which ΔF_{def} was the energy required for cooperative lateral deformation of the incoming and already-tethered disks. ΔF_{def} was made dimensionless by division by kT. When no overlap occurred between

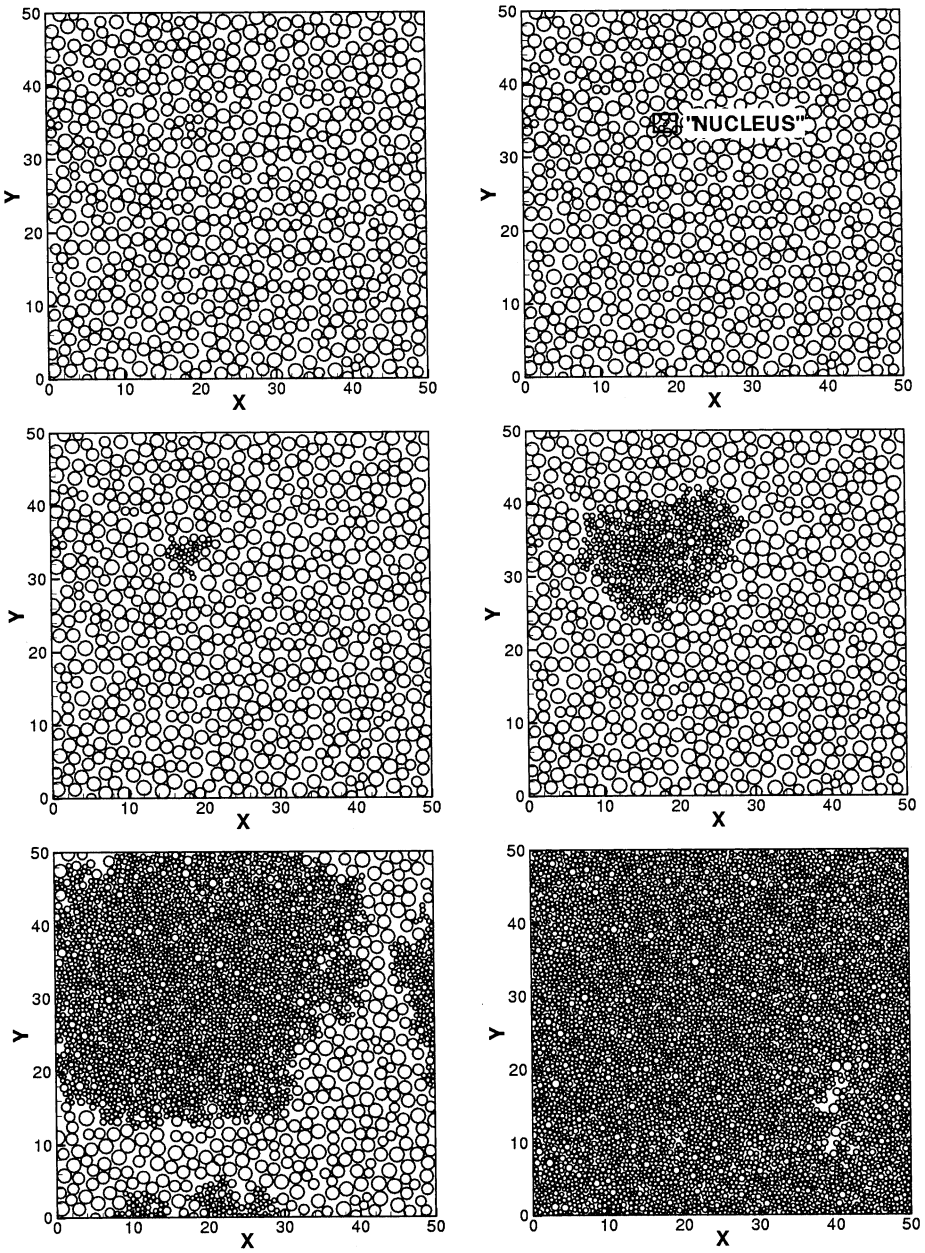

Figure 15. Simulation snapshots of tethered disk configuration at increasing times. Monte Carlo steps are analogous to time in actual tethering. Starting from the upper left, the numbers of MC steps are 17 161, 17 211, 18 391, 20 547, 24 798, and 28 800.

an incoming disk of radius R_g and an already-tethered disk, no deformation was needed and the addition of a new disk was automatically accepted. If the lateral distance between the center of an incoming disk and the center of any of the tethered disks was less than $2R_g$, as it would be for a completed mushroom layer, the energy, ΔF_{def}, required to deform the incoming disk and the disk it overlapped had to be calculated. The deformation energy for a given disk that, in accord with the assumption made in prior studies,[38] had to maintain its circular cross-section parallel to the surface and that was not allowed to overlap another was framed similarly to the confinement energy of a polymer chain confined to a tube of radius less than R_g.[47] The dimensionless deformation energy corresponding to a lateral contraction from an old to a new radius was expressed as

$$\frac{\Delta F_{def}}{kT} = \epsilon\left(\frac{1}{(R_{new}/R_g)^{5/3}} - \frac{1}{(R_{old}/R_g)^{5/3}}\right)$$

where ϵ was a dimensionless quantity that represented the deformation resistance of a disk.

This deformation energy was minimized by setting the radii of both the incoming disk and its nearest already-tethered neighbor to half the distance between their centers. If the incoming disk overlapped with more than one tethered disk, the radii of the other already-tethered disks were reduced until overlap was eliminated. The total energy change for all of the deformations needed for the incoming disk to fit onto the surface was calculated, and the addition of the incoming disk to the surface was accepted according to the Metropolis criterion for Monte Carlo simulations,[48] i.e., with a probability of $e^{-\Delta F_{def}/kT}$. If a disk was not accepted, it was removed, and all the tethered disks surrounding it were restored to their original radii.

Simulations were performed on a two-dimensional flat surface of size $50R_g$ by $50R_g$ with periodic boundary conditions. The dimensionless activation energy, E_{diff}/

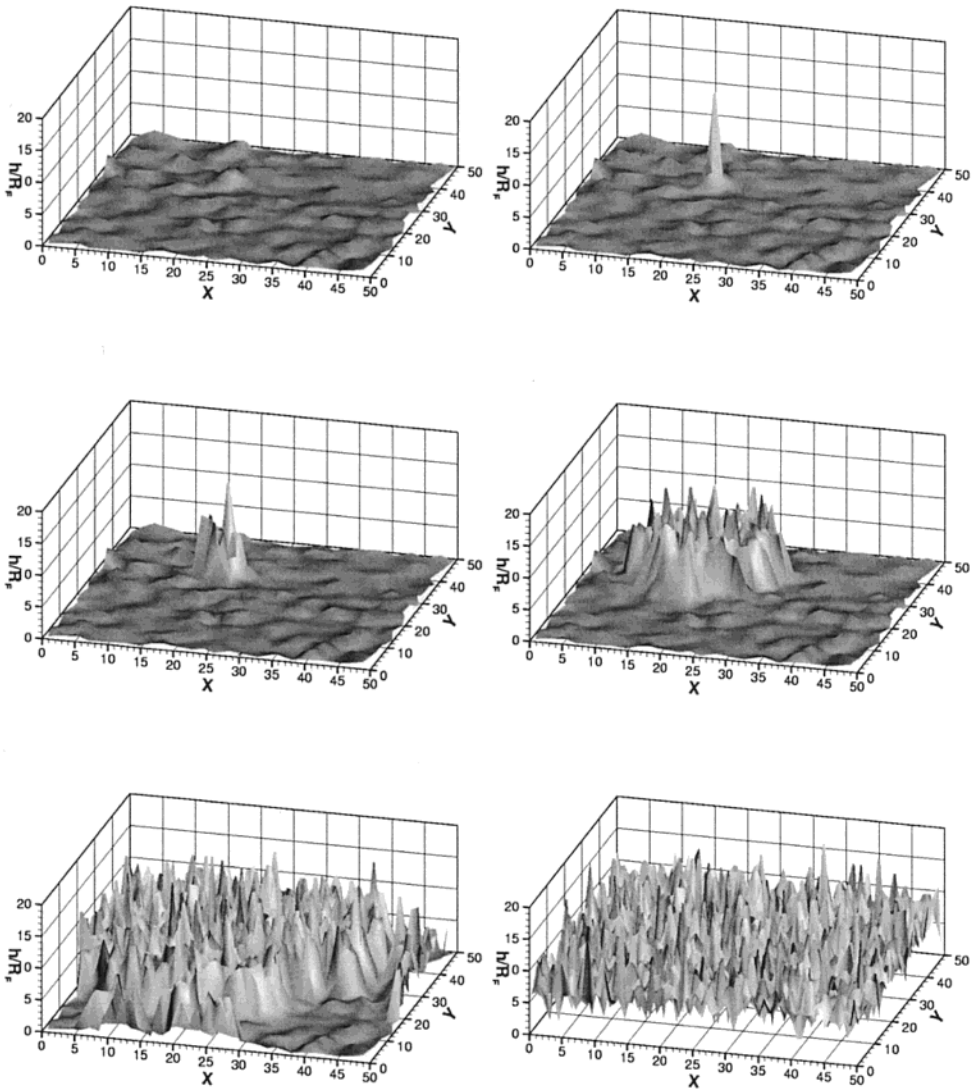

Figure 16. Simulation snapshots of texture (height) of tethered layers at increasing times. Starting from the upper left, the numbers of MC steps are 17 161, 17 211, 18 391, 20 547, 24 798, and 28 800.

kT, for diffusion of an incoming disk into a layer of already-tethered disks was set to 35 and the deformation resistance, ϵ, to 0.5. The results of the simulation are shown in the next three figures.

Figure 14 shows how the averaged quantities vary with steps in the simulation (MC steps), each of which is an attempted addition of a disk to the flat surface. Successive numbers of attempted additions are analogous to passing time (scaled by the average time for subsequent tethering events on the bare surface) in the experimental situation. The most salient feature in this figure is the appearance of three regimes of tethering prior to saturation. In the first regime (<100 MC steps) relaxed disks are able to tether with no energy barrier to the bare surface. In this regime, the fractional coverage of the surface and the normalized attachment density of disks increase linearly with the number of attempted additions. Toward the end of the first regime, the amount of bare surface available for tethering begins to drop, and the diffusion barrier due to already tethered disks becomes important. In the second regime ($100 <$ MC steps $< 2 \times 10^4$), the fractional coverage and attachment density change very slowly and linearly with the log of the number of MC steps. The third regime is the most unexpected, and begins when the attachment density of disks starts to increase rapidly. The rapid increase appears when disks that are already tethered are forced by incoming disks to contract severely. This starts out as a very rare event, but once it begins more space becomes available for additional disks to become tethered, and in turn, exhibit severe lateral contraction. Therefore, the process becomes autoaccelerating (over the relatively large time scale of this regime). Because the lateral size of the disks on the surface decreases rapidly in this regime, the fractional surface coverage actually makes a temporary decrease. This decrease can be seen in Figure 14, and this supports our original speculation of extra space on the surface becoming available as lateral contraction occurs. The curve for normalized surface attachment density in Figure 14 corresponds to the experimental plots in Figures 5−12, except that Figure 14 shows disk addition to the surface, whereas Figures 5−12 show polymer removal from solution.

Our simulation also provided instantaneous snapshots of the configuration of the system around the transition from the second to the third regime of kinetics. These are shown in Figure 15. Just before the transition, the system appears to be more or less jammed, with a relatively narrow distribution of disk

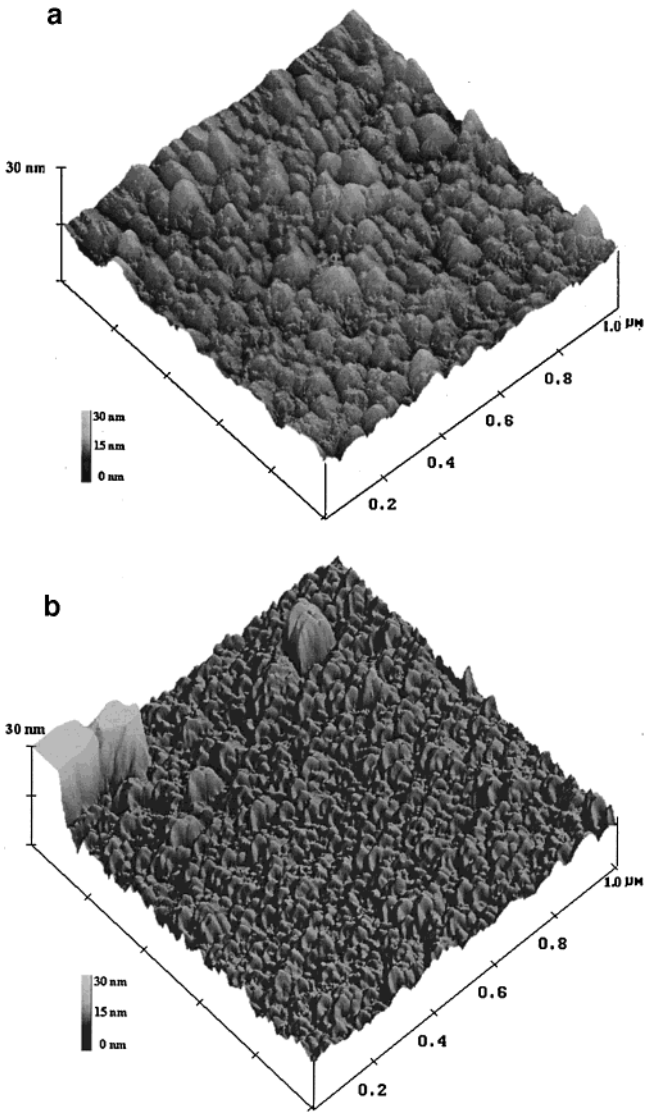

Figure 17. Atomic force microscope images of collapsed polymer layers tethered to glass coverslips. Images were obtained in tapping mode in air, for tethered polystyrene of $M_n = 20\,000$. Key: (a) mushroom layer and (b) brush layer; the latter has more peaks and valleys per unit area than the former.

radii. The critical event that leads to the acceleration of tethering can be seen in the second panel of Figure 15, where one tethered disk is very severely (laterally) contracted near the center of the simulation area. After this, the region of severely contracted disks seems to grow fractally outward from the location of the critical event. Eventually, this region grows to cover the entire simulation area. When a larger simulation area is chosen initially, more critical events arise at random, each generating the kind of dense tethering just described.

This type of process may have interesting consequences for the texture of the tethered layer. The result of our simulation can be compared to those of Douglas et al., who depicted the development of surface texture in a tethered layer.[38] Those authors performed simulations in which only the incoming disks could decrease their radii (and correspondingly extend their lengths to conserve their original volumes) to fit into the spaces between already-tethered disks. In our simulation, we assumed that all of the disks, both incoming and already-tethered, could decrease their radii (and correspondingly extend their lengths to conserve their original volumes). With the further assumptions that the disks each maintained cylindrical shape and were each topped by a hemispherical cap, the scaled height was calculated from

$$\frac{h}{R_g} = \frac{2}{3}\frac{[1 - (R/R_g)^3]}{(R/R_g)^2}$$

where h is height and R is the radius of a given vertically extended disk. Figure 16, a perspective view, shows how the texture evolves at the same set of times depicted in Figure 15. The severely contracted disk that nucleates the change in texture extends much higher than the surrounding tethered layer. As the system evolves, the tethering of additional extended disks and deformation of already tethered disks leads to the propagation of this high spot over the surface of the tethered layer. This process leads to a final brush that has features of much smaller lateral dimensions than those early in the second regime of kinetics.

Figure 17 presents topographical images of the mushroom and brush layers for $M_n = 20\,000$, obtained in air by means of atomic force microscopy in the tapping mode. The surface of the brush layer (Figure 17b) appears to have a greater density of peaks and valleys than the mushroom layer (Figure 17a). A power spectral density analysis of the AFM images was conducted from which the equivalent root-mean-square values for surface roughness were found. The values were 3.45 nm for the mushroom layer and 15.7 nm for the brush layer. A similar analysis was applied to the first and last frames of the images in Figure 16, generated by the Monte Carlo simulation. The values were 0.348 R_g for the first frame and 2.22 R_g for the last frame. The values found by AFM cannot be compared directly with those generated by the Monte Carlo simulation, because the fundamental dimension in the AFM images in the nanometer, while that in the simulation images is radius of gyration, R_g. However, units of dimension can be eliminated by taking ratios, so that the evolution of surface roughness depicted in the AFM images can be compared with that depicted in the simulation images. The ratio for brush over mushroom from the AFM images is 4.6, while the ratio for last frame over first frame in the Monte Carlo image is 6.4. These ratios of root-mean-square surface roughness are within 40% of each other, which is quite good agreement.

It is interesting to consider why the third regime of kinetics has not been reported before. One of the main factors might be a masking effect of concentration or other experimental conditions. For example, conducting tethering reactions from more concentrated solutions (as used by those who construct polymer brushes for physics experiments) might shorten the second regime, making it indistinct from the third and leaving only two regimes of kinetics. This suggestion is supported by our CSA model, which shows that if the parameter E_{diff} is lowered, the second regime becomes considerably shorter.

Before concluding, we wish to point out the practical value of the existence of distinct regimes of kinetic behavior. The change in slope that marks the end of the first regime can be used as a marker by those who want to obtain a mushroom layer instead of a brush. It is now being realized that a mushroom layer is preferable to a brush layer in many applications, such as interfacial

adhesion.[32,49] The second regime, where tethering of additional chains takes place very slowly, provides an opportunity to make mixed layers by adding to the polymer solution or switching solutions while the layer density is relatively constant. Finally, the appearance of the third regime, with the acceleration in tethering rate, signals that saturation has not yet been reached, and that the reaction must be continued.

IV. Conclusion

The kinetics of tethered layer formation by end-functional polystyrene in good solvent was investigated. The data showed three distinct regimes of kinetic behavior rather than the two predicted by theory. The first regime is fast and appears to be controlled by diffusion of polymer through the solvent, as predicted by theory. The second regime is slow and is consistent with dependence on the natural logarithm of time, as predicted by theory. The third regime is one in which tethering accelerates and is not predicted by theory. The acceleration, called layer-assisted tethering, is not fully understood at the present time, and we offer a tentative explanation of it based on cooperative lateral contraction of both incoming and already-tethered polymer chains. A Monte Carlo simulation of a cooperative sequential adsorption process suggested that lateral interactions can explain the acceleration of tethering in the final stages of formation of a polymer brush.

Acknowledgment. This work was supported in part by NSF Grant No. CTS-9911181 and in part by the Research Challenge Trust Fund of the University of Kentucky. K.C. is indebted to NSF Grant No. DMR-9732302 (Research Experiences for Undergraduates). The authors gratefully acknowledge helpful discussions with Dr. Dale W. Schaefer of the University of Cincinnati and with Dr. Jack Douglas of the National Institute of Standards and Technology.

References and Notes

(1) Mansfield, T. L.; Iyengar, D. R.; Beaucage, G.; McCarthy, T. J.; Stein, R. S.; Composto, R. J. Neutron Reflectivity Studies of End-Grafted Polymers. *Macromolecules* **1995**, *28*, 492−499.
(2) Jones, R. A. L.; Norton, L. J.; Shull, K. R.; Kramer, E. J.; Felcher, G. P.; Karim, E. J.; Fetters, L. J. Interfacial Segment Density Profiles of End-Anchored Polymers in a Melt. *Macromolecules* **1992**, *25*, 2359−2368.
(3) Budkowski, A.; Steiner, U.; Klein, J.; Fetters, L. J. Matrix-Modulated Swelling of Polymer Brush. *Europhys. Lett.* **1992**, *20*, 499−504.
(4) Auroy, P.; Auvray, L.; Leger, L. Characterization of the Brush Regime for Grafted Polymer Layers at the Solid−Liquid Interface. *Phys. Rev. Lett.* **1991**, *66*, 719−722.
(5) Dhinojwala, A.; Granick, S. Surface Forces in the Tapping Mode: Solvent Permeability and Hydrodynamic Thickness of Adsorbed Polymer Brushes. *Macromolecules* **1997**, *30*, 1079−1085.
(6) Kumacheva, E.; Klein, J.; Pincus, P.; Fetters, L. J. Brush Formation from Mixtures of Short and Long End-Functionalized Chains in Good Solvent. *Macromolecules* **1993**, *26*, 6477−6482.
(7) Cosgrove, T.; Phipps, J. S.; Richardson, R. M.; Hair, M. L.; Guzonas, D. A. Adsorbed Block Copolymer of Poly(2-vinylpyridine) and Polystyrene by Neutron Reflectivity and Surface Force Techniques. *Macromolecules* **1993**, *26*, 4363−4367.
(8) Penn, L. S.; Hunter, T. F.; Lee, Y.; Quirk, R. P. Grafting Rates of Amine-Functionalized Polystyrenes onto Epoxidized Silica Surfaces. *Macromolecules* **2000**, *33*, 1105−1107.
(9) Dorgan, J. R.; Stamm, M.; Toprakcioglu, C.; Jerome, R.; Fetters, L. J. End-Attaching Copolymer Adsorption: Kinetics and Effects of Chain Architecture. *Macromolecules* **1993**, *26*, 5321−5330.
(10) Motschmann, H.; Stamm, M.; Toprakcioglu, C. Adsorption Kinetics of Block Copolymers from a Good Solvent: A Two-Stage Process. *Macromolecules* **1991**, *24*, 3861−3688.
(11) Huguenard, C.; Varoqui, R.; Pefferkorn, E. Kinetics of Block Copolymer Adsorption. *Macromolecules* **1991**, *24*, 2226−2230.
(12) Tao, J.; Guo, A.; Stewart, S.; Birss, V. I.; Liu, G. Polystyrene-Block-Poly (2-cinnamoylethyl methacrylate) Adsorption in the Buoy-Dominated Regime. *Macromolecules* **1998**, *31*, 172−175.
(13) Budkowski, A.; Losch, A.; Klein, J. Diffusion-Limited Segregation of Diblock Copolymers to a Homopolymer Surface. *Isr. J. Chem.* **1995**, *35*, 55−64.
(14) Ligoure, C.; Leibler, L. Thermodynamics and Kinetics of Grafting End-Functionalized Polymers to an Interface. *J. Phys. (Paris)* **1990**, *51*, 1313−1328.
(15) Hasegawa, R.; Doi, M. Dynamical Mean Field Calculation of Grafting Reaction of End-Functionalized Polymer. *Macromolecules* **1997**, *30*, 5490−5493.
(16) Kramer, E. J. Grafting Kinetics of End-Functional Polymers at Melt Interfaces. *Israel, J. Chemistry* **1995**, *35*, 49−54.
(17) Fredrickson, G. H.; Milner, S. T. Time-Dependent Reactive Coupling at Polymer−Polymer Interfaces. *Macromolecules* **1996**, *29*, 7386−7390.
(18) Fredrickson, G. H. Diffusion-Controlled Reactions at Polymer−Polymer Interfaces *Phys. Rev. Lett.* **1996**, *76*, 3440−3443.
(19) O'Shaughnessy, B.; Sawhney, U. Polymer Reaction Kinetics at Interfaces Interfaces. *Phys. Rev. Lett.* **1996**, *76*, 3444−3447.
(20) Penn, L. S.; Hunter, T. F. A Method for Evaluation of Molecular Weight Distribution of Polydisperse Grafted Layers. *J. Polym. Sci., Part A: Polym. Chem.* **1999**, *37*, 261−265.
(21) Quirk, R. P.; Chen, W.-C. Functionalization of Polymeric Organolithium Compounds. Carbonization. *Makromol. Chem.* **1982**, *183*, 2071−2076.
(22) Gilman, H.; Cartledge, F. K. The Analysis of Organolithium Compounds. *J. Organomet. Chem.* **1964**, *2*, 447−454.
(23) Kruger, C.; Rochow, E. G.; Wannagat, U. Uber die Einwirkung von Natrium-bis-trimethylsilyl-amid auf Benzophenon, Benzaldehyd und Benzochinon. *Chem. Ber.* **1963**, *96*, 2132−2137.
(24) Morton, M.; Fetters, L. J. Anionic Polymerization of Vinyl Monomers. *Rubber Chem. Technol.* **1975**, *48*, 359−365.
(25) Greene, T. W.; Wuts, P. G. M *Protective Groups in Organic Synthesis*, 3rd ed.; Wiley: New York, 1991; p 360.
(26) Fritz, J. S.; Schenk, G. H. *Quantitative Analytical Chemistry*, 3rd ed.; Allyn and Bacon: Boston, MA, 1974.
(27) Ernst-Cabrera, K.; Wilchek, M. Coupling of Ligands to Primary Hydroxyl-Containing Silica for High Performance Affinity Chromatography. *J. Chromatogr.* **1987**, *397*, 187−196.
(28) Hair, M. L.; Tripp, C. P. Alkylchlorosilane Reactions at the Silica Surface. *Colloids Surf. A: Physicochem. Eng. Aspects* **1995**, *105*, 95−103.
(29) Larsson, P. O.; Glad, M.; Hansson, L.; Mansson, M. O.; Ohlson, S.; Mosbach, K. High Performance Liquid Affinity Chromatography. *Advances in Chromatography*; Giddings, J. C., Grushka, E., Cazes, J., Brown, P. R., Eds.; Marcel Dekker: New York, 1983; Vol. 21, pp 41−85.
(30) Guar, R.; Sharma, P.; Gupta, K. 4,4′-Dimethylethoxytrityl Chloride, a Reagent for Spectroscopic Determination of Polymer-Supported Amino Groups. *Analyst* **1989**, *114*, 1147−1150.
(31) Reddy, M.; Rampal, J.; Beaucage, S. An Efficient Procedure for the Solid-Phase Tritylation of Nucleosides and Nucleotides. *Tetrahedron Lett.* **1987**, *28*, 23−26.
(32) Lin, R.; Quirk, R. P.; Kuang, J.; Penn, L. S. Toughening of Impenetrable Interfaces by Monodisperse Tethered Polymer Chains: Effect of Areal Attachment Density. *J. Adhes. Sci. Technol.* **1996**, *10*, 341−349.
(33) Fleer, G. J.; Cohen Stuart, M. A.; Scheutjens, J. M.; Cosgrove, T.; Vincent, B. *Polymers at Interfaces*; Chapman & Hall: London, 1993; Chapter 5.
(34) Parnis, R. Personal communication, University of Connecticut, 2001.
(35) Flory, P. J. *Statistical Mechanics of Chain Molecules*; John Wiley & Sons: New York, 1969; Chapter 1.
(36) Tangari, C.; King, J. S.; Summerfield, G. C. Small-Angle Neutron Scattering on Bulk Polystyrene with Mismatched M_w. *Macromolecules* **1982**, *15*, 132−136.
(37) Schaefer, D. W.; Han, C. C. Quasielastic Light Scattering from Dilute and Semidilute Polymer Solutions. In *Applications of Photon Correlation Spectroscopy*; Pecora, R., Ed.; Plenum Press: New York, 1982; pp 181−243.

(38) Douglas, J. F.; Schneider, H. M.; Frantz, P.; Lipman, R.; Granick, S. The Origin and Characterization of Conformational Heterogeneity in Adsorbed Polymer Layers. *J. Phys.: Condens. Matter* **1997**, *9*, 7699−7718.

(39) Quirk, R. P.; Mathers, R. T. Surface-Initiated Living Anionic Polymerization of Isoprene Using a 1,1-Diphenylethylene Derivative and Functionalization with Ethylene Oxide. *Polym. Bull. (Berlin)* **2002**, *45*, 471−477.

(40) Evans, J. W. Random and Cooperative Sequential Adsorption. *Rev. Modern Phys.* **1993**, *65*, 1281−1329.

(41) Hinrichsen, E. L.; Feder, J.; Jossang, T. Geometry of Random Sequential Adsorption. *J. Stat. Phys.* **1986**, *44*, 793−837.

(42) Talbot, J.; Tarjus, G.; Van Tassel, P. R.; Viot, P. From Car Parking to Protein Adsorption: An Overview of Sequential Adsorption Processes. *Colloids Surf. Sci. A: Phys. Eng. Aspects* **2000** *165*, 287−324.

(43) Milner, S. T.; Witten, T. A.; Cates, M. E. Theory of the Grafted Brush. *Macromolecules* **1988**, *21*, 2610−2619.

(44) Murat, M.; Grest, G. S. Interaction Between Grafted Polymeric Brushes: A Molecular Dynamics Study. *Phys. Rev. Lett.* **1989**, *63*, 1074−1077.

(45) Kopf, A.; Baschnagel, J.; Wittmer, J.; Binder, K. On the Adsorption Process in Polymer Brushes: A Monte Carlo Study. *Macromolecules* **1996**, *29*, 1433−1441.

(46) Zhdanov, V. P.; Kasemo, B. Kinetics of Irreversible Adsorption of Deformable Proteins. *J. Chem. Phys.* **1998**, *109*, 6497−6501.

(47) de Gennes, P. G. *Scaling Concepts in Polymer Physics*; Cornell University Press: Ithaca, NY, 1979.

(48) Metropolis, N.; Rosenbluth, N. A.; Rosenbluth, M. N.; Teller, A. H.; Teller, E. Equation of State Calculations by Fast Computing Machines. *J. Chem. Phys.* **1953**, *21*, 1087−1092.

(49) Brochard-Wyart, F.; de Gennes, P. G.; Leger, L.; Marciano, Y.; Raphael, E. Adhesion Promoters. *J. Phys. Chem.* **1994**, *98*, 9405−9410.

MA020618O